Effects of inertia on conformation and dynamics of tangentially driven active filaments

Mohammad Fazelzadeh [ORCID],[1] Ehsan Irani [ORCID],[2] Zahra Mokhtari,[3] and Sara Jabbari-Farouji[1,*]

[1]*Institute of Physics, University of Amsterdam, 1090 GL Amsterdam, The Netherlands*
[2]*Institute for Theoretical Physics, Georg-August University of Göttingen, Friedrich-Hund Platz 1, 37077 Göttingen, Germany*
[3]*Department of Mathematics and Computer Science, Freie Universität Berlin, Arnimallee 6, 14195 Berlin, Germany*

Active filamentlike systems propelling along their backbone exist across scales ranging from motor-driven biofilaments to worms and robotic chains. In macroscopic active filaments such as a chain of robots, in contrast to their microscopic counterparts, inertial effects on their motion cannot be ignored. Nonetheless, the consequences of the interplay between inertia and flexibility on the shape and dynamics of active filaments remain unexplored. Here we examine inertial effects on a flexible tangentially driven active polymer model pertinent to the above examples and we determine the conditions under which inertia becomes important. Performing Langevin dynamics simulations of active polymers with underdamped and overdamped dynamics for a wide range of contour lengths and activities, we uncover striking inertial effects on conformation and dynamics for high levels of activities. Inertial collisions increase the persistence length of active polymers and remarkably alter their scaling behavior. In stark contrast to passive polymers, inertia leaves its fingerprint at long times by an enhanced diffusion of the center of mass. We rationalize inertia-induced enhanced dynamics by analytical calculations of center-of-mass velocity correlations, applicable to any active polymer model, which reveal significant contributions from active force fluctuations convoluted by inertial relaxation.

I. INTRODUCTION

Active matter systems, consisting of self-driven units, exhibit emergent properties which defy the laws of equilibrium statistical mechanics [1,2]. The majority of recent studies have focused on active particles moving in the realm of low Reynolds numbers, e.g., bacteria and active colloids whose motion is overdamped [2,3]. However, a wide range of macroscopic organisms, including birds, fish, and snakes, as well as synthesized agents such as microflyers [4–6] and shaken granulate chains [7], often have elongated flexible shapes with non-negligible masses which need to be accounted for in the description of their dynamics. Indeed, recent studies have revealed significant inertial effects on the dynamics of individual and collectives of isotropic and rigid active particles [4,6,8–17]. Notably, inertia enhances the diffusive dynamics of active Brownian particles [4,6,16], unlike their passive counterparts, which do not hold any memory of inertia at long times. These findings raise the interesting question of whether inertia induces memory effects and enhanced dynamics for active macroscopic systems with flexible bodies like fish and snakes.

Currently, the consequences of inertia on shape and dynamics of macroscopic active systems remain an open question. To explore the role of inertia on flexible active particles, we consider the widely studied system of linear active filaments [18,19] spanning a diverse range of biological

systems such as biopolymers driven by molecular motors [20,21], worms [22–24], and snakes [25]. Recently, even filamentous robots [24–26] have been achieved, belonging to this class of active systems. Investigations of single overdamped active filaments [18,19,27–31] have revealed that the interplay between activity and flexibility profoundly alters the chain conformation and dynamics and leads to an activity-dependent relaxation time [18,28,32,33]. It also appears that the details of the coupling between the local active force and the conformation of the polymer backbone are crucial for determining the overall dynamics of the polymer. However, it remains unknown under what conditions inertial effects become dominant as we change the scale and mass even if self-propulsion of filaments is governed by the same rules.

Here we examine the inertial effect on the structural and dynamical features of tangentially driven active polymers [27], in which the orientation of the active force on each segment is parallel to the local tangent of the backbone. In this model, the total active force on the polymer is proportional to end-to-end vector; thus the center-of-mass dynamics is directly coupled to the polymer conformation. We focus on this model as recent studies have shown that it provides a good description of several active filaments across the scales including biofilaments driven by molecular motors [27], worms [34], and filamentous robots [26]. Additionally, robotic snakes [35,36] with tangential activity have been realized. The question that arises is for what systems and under what conditions the inertial effects become important. To answer this question, we study the inertial effects on the conformation and dynamics of active filaments of varying contour lengths and activity strengths.

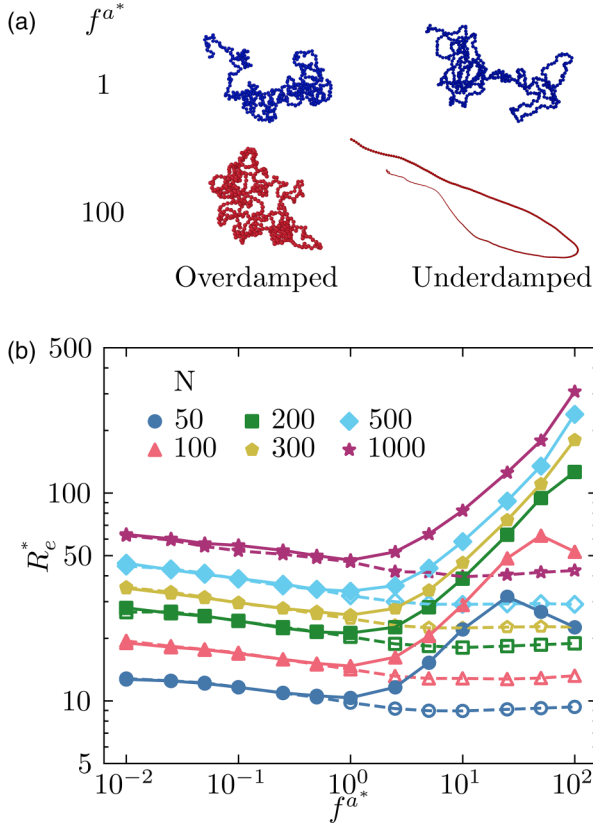*Author to whom correspondence should be addressed: s.jabbarifarouji@uva.nl

FIG. 1. (a) Snapshots of active polymers of size $N = 500$ with active forces $f^{a^*} = 1$ (blue) and 100 (red) in the steady state obtained in the overdamped (left) and underdamped (right) regimes. (b) End-to-end distance R_e^* versus active force f^{a^*} for different chain lengths as given in the legend. The closed and open symbols in (b) correspond to underdamped and overdamped chains, respectively. The lines are guides to the eyes.

Comparing the conformation and dynamics of active polymers in the overdamped and underdamped limits, we find remarkable inertial effects for sufficiently high levels of activity. Inertial effects become non-negligible when the timescale of advection by active force per unit of length becomes smaller than the inertial timescale. At high levels of activity, inertial collisions of active monomers with relative high velocities result in extended chain conformations [see Fig. 1(a)], inducing an activity-dependent persistence length. We find that inertia enhances the diffusive dynamics of the center of mass of inertial active polymers remarkably, in contrast to passive polymers for which inertial effects vanish at long timescales [37–39]. To elucidate the origin of enhanced dynamics, we put forward analytical calculations which derive the center-of-mass velocity time-autocorrelation function in the steady-state limit for an arbitrary active force distribution along a polymer backbone. Our calculations reveal that the enhanced long-time diffusion in any active polymer model stems from fluctuations of the total active force on a filament convoluted by an exponential relaxation with an inertial timescale. For tangentially driven polymers in which the active force is coupled to the polymer conformation, we show that the long-time diffusion coefficient is proportional to the mean-square end-to-end

distance. Hence, our theory illuminates the link between enhanced dynamics and extended polymer conformations.

II. NUMERICAL SIMULATIONS

To further elaborate our insights, we start by outlining our Langevin dynamics simulations of tangentially driven active polymers, implemented in Hoomd Blue software package [40]. The equation of motion for each monomer of an active chain of N beads of mass m in three dimensions is described by

$$m\ddot{\mathbf{r}}_i = -\gamma \dot{\mathbf{r}}_i - \sum_j \nabla_{\mathbf{r}_i} U(r_{ij}) + \mathbf{f}_i^a + \mathbf{f}_i^r, \quad (1)$$

in which $\mathbf{r}_i$ is the coordinate of bead i with the dots denoting derivatives with respect to time, γ is the friction coefficient of the bead with the surrounding medium, and r_{ij} denotes the distance between beads i and j. The potential energy $U(r_{ij})$ includes contributions from harmonic springs of equilibrium length ℓ and stiffness k_s between adjacent monomers and interbead excluded-volume interactions modeled by the WCA potential [41], $U_{\text{excl}}(r) = 4\epsilon[(\frac{\sigma}{r})^{12} - (\frac{\sigma}{r})^6 + \frac{1}{4}]$ for $r < r_c = 2^{1/6}\sigma$. The $\mathbf{f}_i^a$ and $\mathbf{f}_i^r$ are the active and random forces acting on the bead i, respectively. The active force on each bead, except for end monomers, is given by $\mathbf{f}_i^a = \frac{f^a}{2\ell}(\mathbf{r}_{i-1,i} + \mathbf{r}_{i,i+1})$, where $\mathbf{r}_{i,i+1} = \mathbf{r}_{i+1} - \mathbf{r}_i$ defines the bond vector connecting the $(i+1)$th and ith monomers. The active forces on the end monomers are given by $\mathbf{f}_1^a = \frac{f^a}{2\ell}\mathbf{r}_{1,2}$ and $\mathbf{f}_N^a = \frac{f^a}{2\ell}\mathbf{r}_{N-1,N}$. The spring constants are chosen to be very stiff $k_s \gg f^a/\ell$ to ensure that the mean bond length and polymer contour length remain almost constant [see the Supplemental Material (SM) [42] for details]. The random force is chosen as a white noise of zero mean and correlation $\langle \mathbf{f}_i^r(t) \cdot \mathbf{f}_j^r(t') \rangle = 6D_0\gamma^2\delta_{ij}\delta(t-t')$.

We choose $\ell_u = \sigma$, $E_u = \epsilon$, and $\tau_u = \gamma\sigma^2/\epsilon$, with $\gamma = 1$, as the units of length, energy, and time, respectively, denoting reduced quantities with asterisk superscripts. We set $\ell/\sigma = 1$ and the dimensionless diffusion coefficient $D_0^* = 0.1$. To elucidate the role of inertia, we compare the scaling behavior and overall dynamics of underdamped active polymers with $m^* = m\epsilon/(\gamma\sigma)^2 = 1$ and overdamped chains $m^* = 0$, varying the chain length $50 \leqslant N \leqslant 1000$ and active force strength $f^{a^*} = \frac{f^a\sigma}{\epsilon}$ in the range $0.01 \leqslant f^{a^*} \leqslant 100$. Additionally, for chain length $N = 500$ the effects of varying the mass $0 \leqslant m^* \leqslant 5$ on the polymer mean conformation and persistence length are also investigated and included in Fig. 6.

III. RESULTS

A. Inertial effects on conformation

We first investigate inertial effects on the global conformation of polymers. Figure 1(a) shows that the chain conformation is significantly more extended for high active forces in the underdamped scenario. To compare the mean conformation of polymers in the overdamped and underdamped regimes, we plot the end-to-end distance of active polymers, obtained as $R_e^* = \sqrt{\langle \mathbf{R}_e^2 \rangle}/\sigma$, in their steady state as a function of activity f^{a^*} for different chain lengths N as presented in Fig. 1(b). For $f^{a^*} \gg 1$, when the active force per
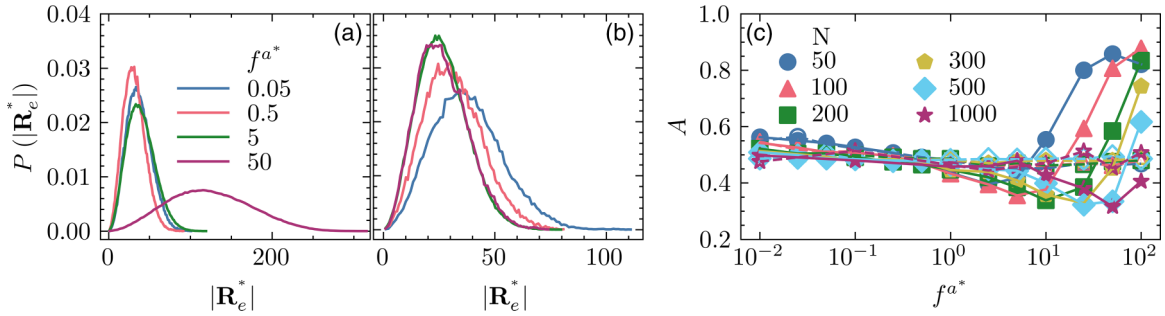
FIG. 2. Probability distribution function of end-to-end distance for active chains of $N = 500$ at different levels of activity with (a) underdamped and (b) overdamped dynamics. (c) Asphericity A of active polymers of different chain lengths $50 \leqslant N \leqslant 1000$ as a function of f^{a^*} in the underdamped (closed symbols) and overdamped (open symbols) regimes.

monomer exceeds the damping force, we observe a striking contrast between conformations of inertial and overdamped active polymers. Chains with underdamped dynamics swell, whereas overdamped chains slightly shrink upon an increase of activity. The onset of departure from the overdamped limit is set by the ratio of the inertial timescale $\tau_{\mathrm{m}} = m/\gamma$ to the time of advection by the active force per monomer $\tau_{\mathrm{adv}} = \sigma\gamma/f^a$. For high active forces when $\tau_{\mathrm{m}}/\tau_{\mathrm{adv}} > 1$, high velocities gained by inertial monomers promote collisions, resulting in chain unwinding. Conformations of inertial chains at higher levels of activity are more extended (see videos in the SM [42]), resulting in a broader probability distribution function of the end-to-end distance $P(|\mathbf{R}_e^*|)$, as can be inferred from Figs. 2(a) and 2(b). For overdamped active chains, we observed a slightly more peaked $P(|\mathbf{R}_e^*|)$ at high levels of activity, reflecting a weak conformational shrinkage. This trend is similar to the observation in Ref. [28], although the degree of shrinkage is much stronger in that work. This is because the model used in our simulations [27] is different from that in Ref. [28], where a different tangential force rule was used [19] and active forces on end beads are switched off. In contrast to the results of Ref. [28], for polymers with overdamped dynamics we do not observe a remarkable coil-globulelike conformational transition upon an increase of activity.

In addition, high-activity inertial chains have more anisotropy in their conformation as evidenced by their larger asphericity, which is defined as [43]

$$A = \frac{\langle \mathrm{Tr}^2 - 3M \rangle}{\langle \mathrm{Tr}^2 \rangle}, \qquad (2)$$

where $\mathrm{Tr} = \lambda_1 + \lambda_2 + \lambda_3$, $M = \lambda_1\lambda_2 + \lambda_2\lambda_3 + \lambda_3\lambda_1$, and each λ is an eigenvalue of the 3×3 gyration tensor. Asphericity ranges from 0 for a perfect spherical conformation to 1 for a rodlike one. Figure 2(c) shows the asphericity A of active polymers against f^{a^*} for chains in the underdamped and overdamped regimes. While A of inertial chains exhibits a striking increase for higher levels of activity, indicating an elongated shape, the asphericity of overdamped chains decreases slightly with f^{a^*}, akin to the trends observed in Ref. [28], albeit much weaker.

To investigate the scaling behavior of active polymers, we analyze the dependence of end-to-end distance on N for different f^{a^*}. Assuming a scaling ansatz $\langle \mathbf{R}_e^{*2} \rangle = C_\infty(f^{a^*})N^{2\nu(f^{a^*})}$, all the data for $N \geqslant 100$ can be collapsed onto a single master

curve (see Fig. 3). The dependence of the scaling exponent ν on f^{a^*} is shown in Fig. 4(a). For $f^{a^*} < 1$, ν drops from $\nu(f^{a^*} = 0.01) = 0.528$ close to that of the self-avoiding walk $\nu_{\mathrm{SAW}} = 0.588$ to the ideal chain exponent $\nu_{\mathrm{ideal}} = \frac{1}{2}$ for both overdamped and underdamped dynamics. At higher levels of activity, when $\tau_m^*/\tau_{\mathrm{adv}}^* = f^{a^*} > 1$ the scaling exponent of overdamped active polymers remains constant within the error bars, whereas for inertial chains the scaling exponent keeps on decreasing even further until $f^{a^*} = 10$ and remains constant afterward, $\nu_{\mathrm{inertial}}(f^{a^*} \gg 1) \approx 0.44$.

The $C_\infty(f^{a^*})$ in the scaling ansatz is a generalized activity-dependent Flory constant which accounts for the conformational rigidity of the polymer backbone. Figure 4(b) shows the extracted C_∞ as a function of f^{a^*} for active polymers with underdamped and overdamped dynamics. Here $C_\infty \sim 1$ up to $f^{a^*} = 1$, whereas for $f^{a^*} > 1$ it remains constant in the case of overdamped polymers; however, it rises steeply for inertial ones. A Flory constant $C_\infty > 1$ implies an increased conformational rigidity compatible with the straighter conformations found for inertial active polymers [see the case of $f^{a^*} = 100$ in Fig. 1(a)]. A reduced ν combined with an increased $C_\infty(f^{a^*})$ for high levels of activity means that the average conformation of inertial active polymers resembles that of compact globulelike polymers with a large persistence length.
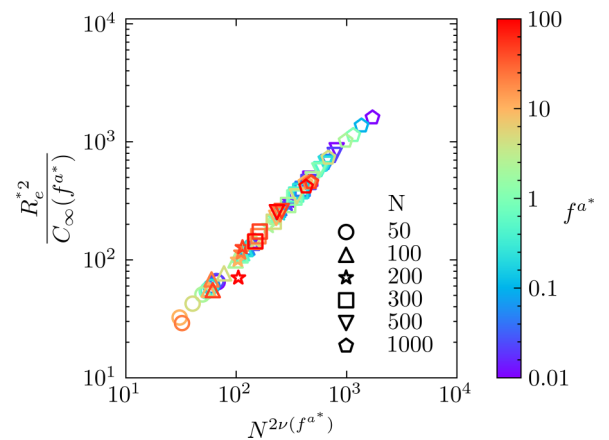

FIG. 3. Normalized $\frac{R_e^{*2}}{C_\infty(f^{a^*})}$ as a function of $N^{2\nu(f^{a^*})}$ for underdamped chains. We exclude the outliers of R_e^*, which are $(N, f^{a^*}) \in \{(50, 50), (50, 100), (100, 100)\}$.
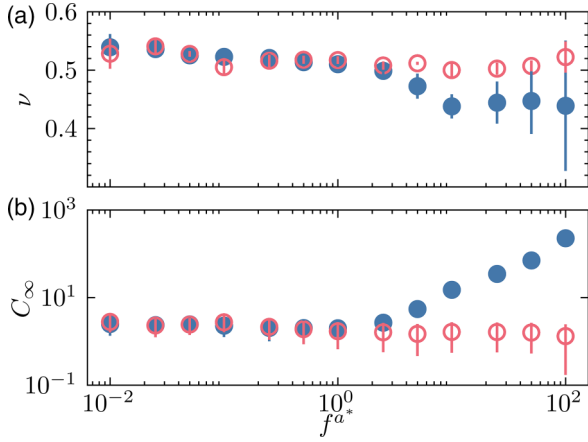
FIG. 4. (a) Scaling exponent ν of end-to-end distance and (b) generalized Flory constant C_∞ as a function of f^{a^*}, assuming $R_e^{*2}(N, f^{a^*}) = C_\infty(f^{a^*})N^{2\nu(f^{a^*})}$. The closed and open symbols correspond to underdamped and overdamped chains, respectively.

A growing C_∞ also implies an increasing persistence length with f^{a^*}. To obtain the persistence length, we compute the orientational bond-bond correlation function $\langle\cos\theta(s)\rangle$ defined as the cosine of the angle between any two bonds whose curvilinear distance is s. Figures 5(a) and 5(b) present $\langle\cos\theta(s)\rangle$ against curvilinear distance s along the polymer backbone at different levels of activity for inertial and overdamped chains, respectively. For both cases, the bond-bond correlation function develops a negative dip at intermediate s, indicating a local backfolding of active chains. For inertial chains, the bond orientational correlation along the backbone becomes larger upon an increase of activity and the negative dip appears at larger s, whereas for overdamped active chains the decay length is weakly affected by activity. The $\langle\cos\theta(s)\rangle$ does not decay exponentially. Nonetheless, we choose to define the persistence length ℓ_p^* as the curvilinear distance at which $\langle\cos\theta(\ell_p^*)\rangle = 1/e$. The extracted persistence lengths ℓ_p^* for overdamped and inertial chains versus f^{a^*} are presented in Fig. 5(c) and show identical trends for different N. For overdamped polymers, ℓ_p^* remains unity up to $f^{a^*} \sim 1$ and increases slightly beyond it, whereas for inertial polymers ℓ_p^* increases steeply with f^{a^*} when $\tau_m^*/\tau_{\rm adv}^* > 1$.

The inertia-induced persistence length at high levels of activity scales linearly with f^{a^*} and it can be interpreted as

the distance at which an active monomer travels by speed $v^{a^*} = f^{a^*}/\gamma^*$ during the inertial timescale τ_m^* giving rise to $\ell_p \sim f^{a^*} m^*/\gamma^{*2}$ yielding $\ell_p^* \sim f^{a^*} m^*$. For $N = 50$ and 100, ℓ_p^* exhibits a decrease when the contour length becomes comparable to the persistence length $\ell_p^* \sim N$ and it cannot grow anymore; hence a new instability appears. Overall, we recognize a similar trend for ℓ_p^* and C_∞ against the active force, corroborating the surmise of an inertia-induced bending rigidity in active polymers. We emphasize that locally straight conformations arise due to the interplay between inertia and activity. Neither the tangential driving force nor inertia alone leads to locally straight chain conformations as evidenced by the ℓ_p^* plot in Fig. 5(c). To verify our suggested scaling for the activity-dependent persistence length $\ell_p^* \sim f^{a^*} m^*$ for high levels of activity, we vary both the mass and active force for a fixed chain length $N = 500$. Figure 6(a) shows the persistence length as a function of $m^* f^{a^*}$ and confirms that ℓ_p^* varies linearly with $m^* f^{a^*}$ when $1 \leqslant m^* f^{a^*} \leqslant 100$. For smaller values of $m^* f^{a^*}$ the relation is nonlinear because $\tau_m^* < \tau_{\rm adv}^*$ and the inertial effects are not dominant. On the other extreme of large $m^* f^{a^*}$, we observe a deviation from linear scaling because the magnitude of the persistence length becomes comparable to the chain length $N = 500$. At this range of activity and mass the end-to-end distance reaches its largest possible value ($R_e^* = N = 500$), as shown in Fig. 6(b) for the chains with $f^{a^*} \geqslant 50$ and $m^* \geqslant 3$.

B. Inertial effects on dynamics

Having explored the inertial effects on structural features of active polymers, we examine the signatures of inertia on the dynamics. We start by investigating the polymer orientational dynamics. To this end, we compute the time-autocorrelation function (TACF) of the end-to-end vector normalized by its mean-square value in the steady-state limit $\hat{C}_e(t) = \lim_{t'\to\infty}\langle\mathbf{R}_e(t + t')\cdot\mathbf{R}_e(t')\rangle/\langle\mathbf{R}_e^2(t')\rangle$. As the total active force $\mathbf{F}^a$ is proportional to the end-to-end vector $\mathbf{F}^a = \sum_{i=1}^{N}\mathbf{f}_i^a = \frac{f^a}{\ell}\mathbf{R}_e$, the relaxation time of $\hat{C}_e$ is identical to the persistence time of the total active force. Figure 7(a) shows $\hat{C}_e$ at different activity levels for inertial and overdamped chains of length $N = 500$. Although for large f^{a^*} the $\hat{C}_e(t)$ of inertial chains exhibits a decay with oscillatory behavior, the overall decorrelation timescales of $\hat{C}_e(t)$ of the two kinds of dynamics are very similar, in contrast to the huge difference in their chain conformations. This trend suggests that we have
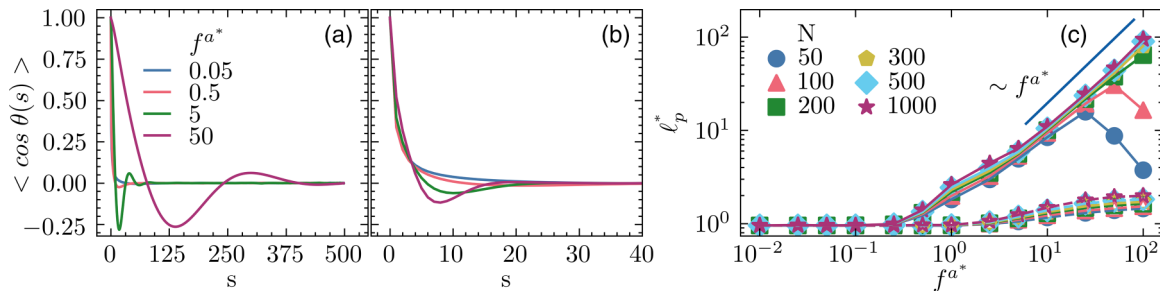

FIG. 5. Bond-bond orientational correlation function against curvilinear distance s for (a) inertial and (b) overdamped chains with $N = 500$ at different levels of activity. (c) Dependence of persistence length ℓ_p^* on f^{a^*} for inertial (closed symbols) and overdamped (open symbols) polymers of different lengths.
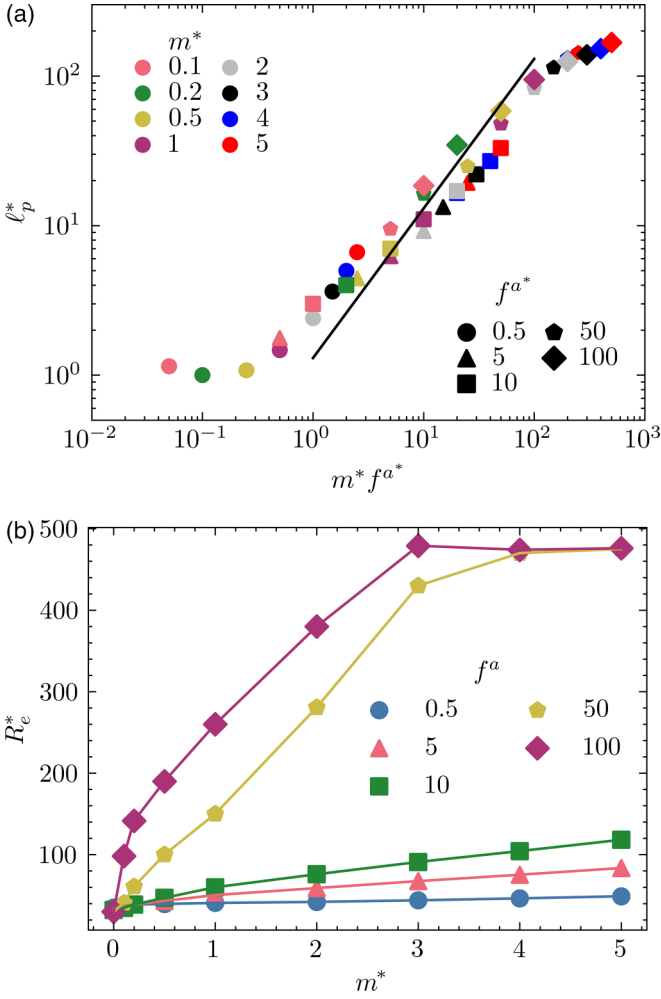
FIG. 6. (a) Persistence length of active chains of length $N = 500$ with different masses and activity levels as a function of their mass times their active force $m^* f^{a^*}$. The solid line shows a fit with a slope of 1 for the data within $1 \leqslant m^* f^{a^*} \leqslant 100$. (b) End-to-end distance against mass for chains with $N = 500$ and various activities.

a universal relaxation time $\tau_e(N, f^a)$, which depends only on the strength of the active force and the chain length and is independent of the mass. We find that the initial decay of $\hat{C}_e(t)$ for both overdamped and underdamped polymers can be approximately described by an exponential function (see Fig. S2 in [42]). The extracted relaxation times τ_e^* [shown in Fig. 7(b)] follow the scaling relation

$$\tau_e^*(N, f^{a^*}) \approx 0.6N/f^{a^*}, \qquad (3)$$

verifying that activity reduces the relaxation time as $1/f^{a^*}$ and also the dependence of the relaxation time on the chain length becomes linear, which is weaker than the $N^{1+2\nu}$ dependence for the self-avoiding Rouse model [44]. These findings are in agreement with those reported in Ref. [28] for overdamped active polymers.

We subsequently compute the TACF of the center-of-mass velocity normalized by the long-time mean-square velocity of the center of mass in the steady-state limit $\hat{C}_v(t) = \lim_{t' \to \infty} \langle \mathbf{V}_{\text{c.m.}}(t + t') \cdot \mathbf{V}_{\text{c.m.}}(t') \rangle / \langle \mathbf{V}_{\text{c.m.}}^2(t') \rangle$, where
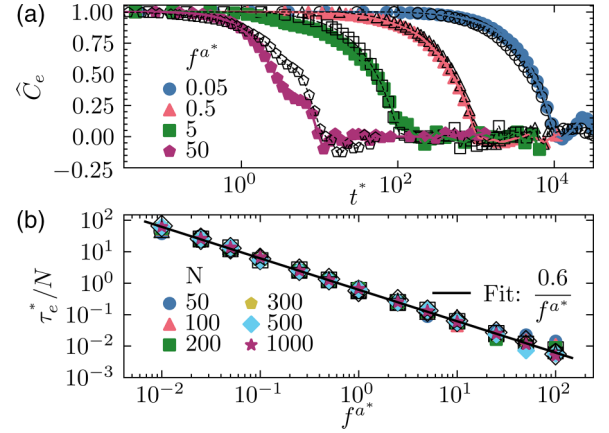

FIG. 7. (a) Normalized end-to-end vector TACF $\hat{C}_e$ as a function of time t for inertial (closed symbols) and overdamped (open black symbols) chains of $N = 500$ at different levels of activity. (b) Corresponding relaxation times divided by chain length against active force for inertial (closed symbols) and overdamped (open black symbols) polymers, extracted from fitting the initial decay of $\hat{C}_e(t)$ with the exponential function.

$\mathbf{V}_{\text{c.m.}}(t) = \frac{1}{N} \sum_{i=1}^{N} \mathbf{v}_i$. Figures 8(a) and 8(b) show $\hat{C}_v$ for underdamped and overdamped active polymers of $N = 500$ at different f^{a^*}, respectively. Unlike passive systems, we observe a finite relaxation of $\hat{C}_v$ even for the overdamped dynamics manifesting the contribution of active forces on velocity correlations. For the underdamped active chains, we recognize an initial fast decay with a relaxation time $\tau_m^* = 1$ in addition to a longer decay time which is similar to that of the overdamped chains. For both kinds of dynamics, the characteristic relaxation times of $\hat{C}_v$ decrease with f^{a^*}, similar to trends observed for $\hat{C}_e$. In Figs. 8(c) and 8(d) we have present $\langle \mathbf{V}_{\text{c.m.}}^{*2} \rangle$ as a function of f^{a^*} for underdamped and overdamped dynamics, respectively. For inertial chains,
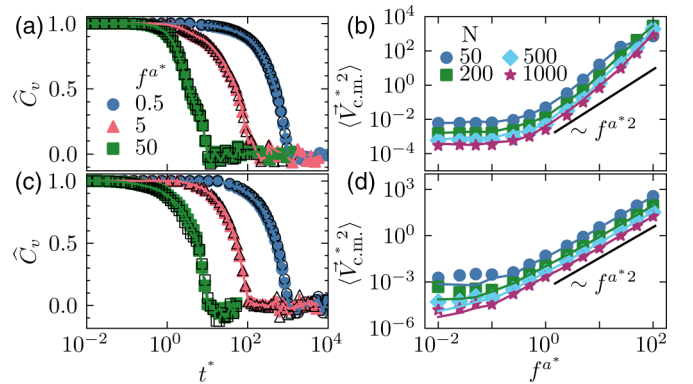

FIG. 8. Normalized center-of-mass velocity TACF for (a) inertial and (b) overdamped active polymers of $N = 500$ and different activity levels. The closed symbols are obtained directly from simulations, whereas open black ones are calculated using Eqs. (6) and (7) with C_e as input from simulations. Also shown is the mean-square velocity of the center of mass of different chain lengths as given in the legends versus f^{a^*} for (c) inertial and (d) overdamped active polymers. The lines show theoretical predictions of Eqs. (9) and (10).
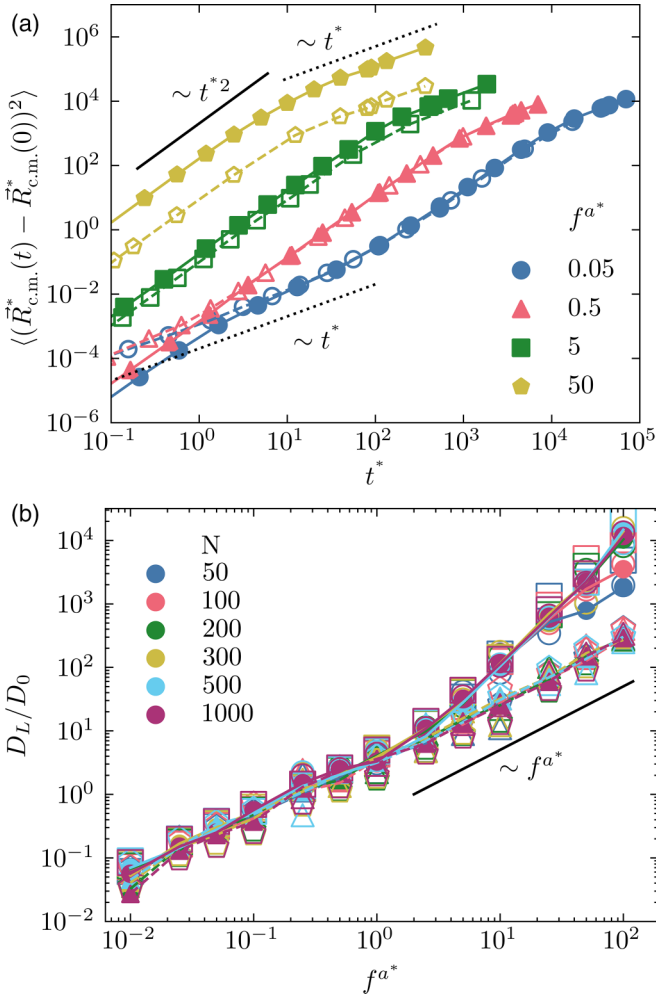
FIG. 9. (a) Mean-square displacement of the center of mass for chains of $N = 500$ and different levels of activity for underdamped (closed) and overdamped (open) polymers. (b) Long-time diffusion coefficient D_L of the center of mass normalized by monomer diffusion D_0 against f^{a^*} for active polymers of chain lengths $50 \leqslant N \leqslant 1000$ in the underdamped (closed circles) and overdamped (closed triangles) regimes. The open circles and triangles show predictions of Eqs. (11) and (12), receptively, using the end-to-end vector TACF from simulations. The squares and pentagons display the predictions of Eq. (13), assuming $\tau_e^* = 0.6N/f^{a^*}$.

the mean-square velocity is almost independent of f^{a^*} for $f^{a^*} < 1$, whereas for large active forces it grows steeper than f^{a^*2}. In the overdamped scenario, we observe a weak decrease of $\langle \mathbf{V}_{\text{c.m.}}^{*2} \rangle$ for small f^{a^*} but it grows as f^{a^*2} for higher levels of activity. Nevertheless, the mean-square velocities of inertial chains for high levels of activity are one order of magnitude larger.

Finally, we investigate the mean-square displacement (MSD) of the center of mass as presented in Fig. 9(a) for the active chains of length $N = 500$ with overdamped and underdamped dynamics at different activity levels. For low levels of activity $f^{a^*} < 1$, the MSDs of the two scenarios at times $t^* > 1$ coincide. After an initial short-time diffusive (overdamped) or ballistic (underdamped) regime, the MSDs exhibit a superdiffusive regime induced by activity, followed

by a long-time diffusion in agreement with the results reported in [28] for overdamped active polymers. However, at higher levels of activity $f^{a^*} \geqslant 5$, the MSDs of two scenarios start to depart and we observe a remarkably faster dynamics for underdamped chains. At high levels of activity the MSDs of both underdamped and overdamped chains exhibit a crossover from ballistic regime directly to diffusive regime. We extract the long-time diffusion coefficient of center of mass D_L from the slope of mean-square displacement at large times, i.e., $t^* > \tau_e^*$. Figure 9(b) shows D_L versus f^{a^*} for inertial and overdamped chains. Intriguingly, two distinct sets of curves for inertial and overdamped chains emerge and the long-time diffusion of inertial chains at high levels of activity is two orders of magnitude larger. Notably, D_L is almost independent of chain length, in contrast to passive polymers for which $D_L \sim 1/N$ [45], depending mainly on f^{a^*} and mass. Our results in the overdamped limit are consistent with an earlier reports of reference [28] but clearly show that inertia leads to additional enhancement of the long-time dynamics of active polymers and raise questions about its origin. To rationalize the remarkable enhancement of dynamics, we put forward analytical calculations which illuminate the relationship between TACFs of the center-of-mass velocity and the total active force $\mathbf{F}^a$ in the steady-state limit for any active polymer model as presented in the following subsection. Then, we will compare theoretical predictions with our simulation results for the tangentially driven polymers.

C. Analytical calculations of center-of-mass dynamics

The dynamics of the center-of-mass velocity $\mathbf{V}_{\text{c.m.}}(t)$ is obtained by summing the equations of motions of all the beads given by Eq. (1). As contributions from the internal forces cancel out, the equation for $\mathbf{V}_{\text{c.m.}}(t)$ simplifies to

$$m\dot{\mathbf{V}}_{\text{c..m}} = -\gamma \mathbf{V}_{\text{c.m.}} + \frac{1}{N}(\mathbf{F}^a + \mathbf{F}^r), \quad (4)$$

in which $\mathbf{F}^r = \sum_{i=1}^N \mathbf{f}_i^r$ is a sum of all the random forces with a zero mean and $\langle \mathbf{F}^r(t) \cdot \mathbf{F}^r(t') \rangle = 6ND_0\gamma^2\delta(t - t')$. Integrating this first-order differential equation yields

$$\mathbf{V}_{\text{c.m.}}(t) = \mathbf{V}(t_0)e^{-(\gamma/m)(t-t_0)}$$

$$+ \frac{1}{Nm}\int_{t_0}^t d\tau[\mathbf{F}^a(\tau) + \mathbf{F}^r(\tau)]e^{-(\gamma/m)(t-t_0-\tau)}. \quad (5)$$

Using this solution, we calculate the velocity TACF in the steady-state limit, defined as $C_v(t) = \lim_{t' \to \infty}\langle \mathbf{V}_{\text{c.m.}}(t + t') \cdot \mathbf{V}_{\text{c.m.}}(t') \rangle$, yielding

$$C_v(t) = \frac{3\gamma D_0}{Nm}e^{-t/\tau_m}$$

$$+ \frac{1}{2m\gamma N^2}\int_0^{+\infty}[C_f(u - t) + C_f(u + t)]e^{-u/\tau_m}du, \quad (6)$$

in which $C_f(t) = \lim_{t' \to \infty}\langle \mathbf{F}^a(t + t') \cdot \mathbf{F}^a(t') \rangle$ is the TACF of the total active force. The first term in Eq. (6) represents the passive diffusive contribution from random forces, which decays exponentially with the relaxation time τ_m [37], whereas the second term entangles the correlation of the total active force with the inertial relaxation. This term reflects memory

effects induced by active forces and accounts for the emergent inertial effects. We emphasize that Eq. (6) is derived without making any assumption about the form of the active force distribution along the polymer backbone in terms of both magnitude and orientation, i.e., being tangential, transverse, or random. Hence, this result is applicable to any active polymer model.

In the limit of vanishing mass, C_v simplifies to

$$\lim_{m \to 0} C_v(t > 0) = \left(\frac{1}{N\gamma}\right)^2 C_f(t). \tag{7}$$

Concerning tangentially driven polymers, for which the total active force $\mathbf{F}^a = f^a \mathbf{R}_e / \ell$ is directly coupled to the chain conformation, the total force correlation is $C_f(t) = (f^{a2} \langle R_e^2 \rangle / \ell^2) \hat{C}_e(t)$. The predictions of Eqs. (6) and (7) when normalized by their values at $t^* = 0$ show excellent agreement with velocity correlations computed from simulations, as demonstrated in Figs. 8(a) and 8(b).

For an active force TACF with exponential decay $C_f = A_f e^{-t/\tau_f}$, Eq. (6) simplifies to

$$C_v(t) = \frac{3\gamma D_0}{Nm} e^{-t/\tau_m}$$
$$+ \frac{A_f^2}{(Nm)^2} \left(\frac{\tau_m^2 \tau_f}{\tau_f^2 - \tau_m^2}\right)(\tau_f e^{-t/\tau_f} - \tau_m e^{-t/\tau_m}), \tag{8}$$

which consists of exponential decays at two timescales: the inertial time τ_m and the decay time of the active force TACF τ_f. In this case, the center-of-mass velocity TACF of active polymers becomes identical to that of the inertial active Ornstein-Uhlenbeck model [11,16]. The approximation of the exponential decay of the active force TACF becomes exact in the case of an active Brownian polymer model [32,46] with only translational inertia (see Sec. III in the SM [42]). As discussed earlier, $\hat{C}_e(t)$ approximately follows an exponential decay. Thus, Eq. (8) also provides a good description of tangentially driven active polymers provided we consider an activity-dependent amplitude A_f which is coupled to the polymer mean conformation.

We can also obtain the steady-state mean-square center-of-mass velocity for tangentially driven polymers from Eq. (6), yielding

$$\lim_{t \to \infty} \langle \mathbf{V}_{\text{c.m.}}^2(t) \rangle$$
$$= \frac{3\gamma D_0}{Nm} + \frac{f^{a2}}{m\gamma N^2} \frac{\langle R_e^2 \rangle}{\ell^2} \int_0^{+\infty} \hat{C}_e(u) e^{-u/\tau_m} du, \tag{9}$$

which for small f^a is dominated by the diffusive term, whereas when $\frac{f^{a2}}{3N\gamma^2 D_0} \frac{\langle R_e^2 \rangle}{\ell^2} > 1$ it is determined by the active contribution. For sufficiently large f^a such that the relaxation time $\tau_e < \tau_m$, $\int_0^{+\infty} \hat{C}_e(u) e^{-u/\tau_m} du \approx \tau_e$. In this limit, $\langle \mathbf{V}_{\text{c.m.}}^2 \rangle (f^a \gg 1) = \frac{f^{a2}}{m\gamma N^2} \frac{\langle R_e^2 \rangle}{\ell^2} \tau_e$. Using Eq. (3) and the scaling behavior of $\langle R_e^2 \rangle$, it becomes proportional to $f^{a2} N^{2\nu(f^a)-1}$. Equation (9) in the limit of vanishing mass simplifies to

$$\lim_{m \to 0} \langle \mathbf{V}_{\text{c.m.}}^2(t \gg 1) \rangle = \frac{f^{a2} \langle R_e^2 \rangle}{(\ell^2 N\gamma)^2}. \tag{10}$$

A comparison of Eqs. (9) and (10) with $\langle \mathbf{V}_{\text{c.m.}}^{*2}(0) \rangle$, presented in Figs. 8(c) and 8(d), shows very good agreement.

The explicit form of the TACF of velocity given by Eq. (6) allows us to predict the long-time diffusion of the center of mass by integrating it over time: $D_L = \frac{1}{3} \int_0^\infty dt\, C_v(t)$. For inertial tangentially driven polymers, this yields

$$D_L = \frac{D_0}{N} + \frac{f^{a2} \langle R_e^2 \rangle}{6m\gamma N^2 \ell^2}$$
$$\times \int_0^{+\infty} dt \int_0^{+\infty} [\hat{C}_e(u - t) + \hat{C}_e(u + t)] e^{-u/\tau_m} du. \tag{11}$$

For the overdamped chains, in the limit of $m \to 0$, Eq. (11) simplifies to

$$D_L = \frac{D_0}{N} + \frac{f^{a2} \langle R_e^2 \rangle}{3\gamma^2 N^2 \ell^2} \int_0^{+\infty} dt\, \hat{C}_e(t), \tag{12}$$

yielding results identical to the calculations in Ref. [28]. The predictions of Eqs. (11) and (12) are shown in Fig. 9(b) by open circles and triangles, respectively, demonstrating excellent agreement with simulation results. Approximating $\hat{C}_e(t)$ with an exponential function $\hat{C}_e(t) = e^{-t/\tau_e}$ and using Eq. (3) for the relaxation time, Eqs. (11) and (12) yield an identical approximate equation for inertial and overdamped systems

$$D_L \approx \frac{D_0}{N} + \frac{f^{a2} \langle R_e^2 \rangle \tau_e}{3N^2 \gamma^2 \ell^2}. \tag{13}$$

This equation clarifies that the inertia-induced enhancement of D_L originates from extended chain conformations generating an overall larger $\langle R_e^2 \rangle$. Assuming $\tau_e \sim N/f^a$, the long-time diffusion scales as $D_L \sim N^{2\nu - 1}$, which weakly depends on N. Hence, this equation shows that at sufficiently high levels of activity the dominant contribution in D_L comes from activity. We note that in the overdamped limit, $\langle R_e^2 \rangle$ becomes independent of activity for large active forces [see Fig. 1(b)] and given that $\nu \approx 0.5$, D_L becomes independent of N and varies linearly with f^a in agreement with prior simulation results of a similar model [28] and analytical calculations for tangentially driven Gaussian polymers [33,47]. A comparison of simulation results with Eq. (13) is also included in Fig. 9(b), revealing good agreement and verifying the approximate relation between D_L, $\langle R_e^2 \rangle$, and τ_e.

IV. CONCLUSION

We have combined bead-spring simulations and analytical theory to provide insights into the fundamental interplay between inertia, activity, and flexibility in tangentially driven active filaments. For this model, active forces are coupled to polymer conformations and inertia conspicuously affects both conformational and dynamical features. Inertial effects become significant when the inertial timescale of a monomer (active unit) $\tau_m = m/\gamma$ become longer than the timescale of its advection by an active force $\tau_{\text{adv}} = \sigma\gamma/f^a = \sigma/v^a$ causing a delay between the end-to-end vector and center-of-mass velocity. Inertial collisions of high-speed monomers cause extended conformations, hence increasing the persistence length of polymers. The chain unwinding in turn result

in an enhanced mean velocity and diffusion of the center of mass, as elucidated by our theoretical analysis. The analytical calculations show that for tangentially driven polymers, the key quantity determining the enhanced dynamics in active polymers was the ratio of the end-to-end distance to contour length.

Having determined the conditions under which inertial effects become dominant, we conclude that for active biopolymers such as molecular-motor-driven actin and myosin the inertial effects are negligible even for the highest activity levels $f^{a^*} \sim 100$. However, for sufficiently heavy robotic filaments moving in a low-friction medium, e.g., a chain of small self-propelling robotic toys or drones, inertial effects become important and should be taken into account. As an illustration, consider a robotic filament made of small self-propelling toys [26]. According to Ref. [48], the measured inertial relaxation time for a unit is $\tau_m \approx 0.1$ s and each bot of length $\sigma = 0.04$ m has a self-propulsion velocity of $v_a = f^a/\gamma \approx 0.2$ m/s, leading to an active advection timescale $\tau_{adv} = \sigma/v^a \approx 0.2$ s. For a robotic filament made from these bots, $\tau_m/\tau_{adv} \sim 5$ is significantly large and inertia influences the mean conformation and long-time dynamics of filaments. As such, our study provides a guideline for the design of active robotic filaments.

It is worth mentioning that although we focused on a flexible, active, tangentially driven polymer model, our analytical calculations are applicable to any force-driven active polymer model. As such, these results give the conditions under which inertia affects long-time dynamics. For example, for the active Brownian polymer model [32], our analysis reveals that inertial effects on long-time dynamics become relevant when rotational inertia is sufficiently large. Moreover, the results of our study should inspire investigation of a deeper link between memory effects and inertia in the collective dynamics of active filaments and more generally other active systems with internal degrees of freedom. We conclude our paper with a final remark. Given the significant effects of inertia on the conformation and long-time dynamics of tangentially driven active filaments, the ratio of the mass to the damping coefficient in simulations of active polymers with inertial terms [40,49,50] should be chosen carefully to ensure that they capture the correct inertial or overdamped regime.

[1] S. Ramaswamy, Annu. Rev. Condens. Matter Phys. **1**, 323 (2010).

[2] M. C. Marchetti, J. F. Joanny, S. Ramaswamy, T. B. Liverpool, J. Prost, M. Rao, and R. A. Simha, Rev. Mod. Phys. **85**, 1143 (2013).

[3] P. Romanczuk, M. Bär, W. Ebeling, B. Lindner, and L. Schimansky-Geier, Eur. Phys. J.: Spec. Top. **202**, 1 (2012).

[4] C. Scholz, S. Jahanshahi, A. Ldov, and H. Löwen, Nat. Commun. **9**, 5156 (2018).

[5] J. Rogers, B. H. Kim, K. Li, J.-T. Kim, Y. Park, H. Jang, X. Wang, Z. Xie, S. Won, W. Jang, K. Lee, T. Chung, Y. H. Jung, S. Heo, Y. Lee, J. Kim, C. Tengfei, Y. Kim, P. Prasopsukh, Y. Zhang *et al.*, Nature **597**, 503 (2021).

[6] H. Lowen, J. Chem. Phys. **152**, 040901 (2020).

[7] K. Safford, Y. Kantor, M. Kardar, and A. Kudrolli, Phys. Rev. E **79**, 061304 (2009).

[8] K. Malakar, A. Das, A. Kundu, K. V. Kumar, and A. Dhar, Phys. Rev. E **101**, 022610 (2020).

[9] S. Jahanshahi, Microswimmers and microflyers in various complex environments, Ph.D. thesis, Heinrich Heine Universität Düsseldorf, 2019.

[10] R. Chatterjee, N. Rana, R. A. Simha, P. Perlekar, and S. Ramaswamy, Phys. Rev. X **11**, 031063 (2021).

[11] L. Caprini and U. M. B. Marconi, J. Chem. Phys. **154**, 024902 (2021).

[12] M. Sandoval, Phys. Rev. E **101**, 012606 (2020).

[13] L. L. Gutierrez-Martinez and M. Sandoval, J. Chem. Phys. **153**, 044906 (2020).

[14] C. Dai, I. R. Bruss, and S. C. Glotzer, Soft Matter **16**, 2847 (2020).

[15] A. R. Sprenger, S. Jahanshahi, A. V. Ivlev, and H. Löwen, Phys. Rev. E **103**, 042601 (2021).

[16] G. H. Nguyen, R. Wittmann, and H. Löwen, J. Phys.: Condens. Matter **34**, 035101 (2021).

[17] L. Caprini, R. K. Gupta, and H. Löwen, Role of rotational inertia for collective phenomena in active matter, Phys. Chem. Chem. Phys. **24**, 24910 (2022).

[18] R. G. Winkler, J. Elgeti, and G. Gompper, J. Phys. Soc. Jpn. **86**, 101014 (2017).

[19] R. G. Winkler and G. Gompper, J. Chem. Phys. **153**, 040901 (2020).

[20] B. Alberts, *Molecular Biology of the Cell* (TPB, Beaumont, 2007).

[21] D. Bray, *Cell Movements: From Molecules to Motility*, 2nd ed. (Garland Science, New York, 2001).

[22] A. Deblais, A. C. Maggs, D. Bonn, and S. Woutersen, Phys. Rev. Lett. **124**, 208006 (2020).

[23] A. Deblais, S. Woutersen, and D. Bonn, Phys. Rev. Lett. **124**, 188002 (2020).

[24] Y. Ozkan-Aydin, D. Goldman, and S. Bhamla, Proc. Natl. Acad. Sci. USA **118**, e2010542118 (2021).

[25] H. Marvi, C. Gong, N. Gravish, H. Astley, M. Travers, R. L. Hatton, J. R. Mendelson, H. Choset, D. L. Hu, and D. I. Goldman, Science **346**, 224 (2014).

[26] E. Zheng, M. Brandenbourger, L. Robinet, P. Schall, E. Lerner, and C. Coulais, Self-oscillation and synchronisation transitions in elasto-active structures, Phys. Rev. Lett. **130**, 178202 (2023).

[27] R. E. Isele-Holder, J. Elgeti, and G. Gompper, Soft Matter **11**, 7181 (2015).

[28] V. Bianco, E. Locatelli, and P. Malgaretti, Phys. Rev. Lett. **121**, 217802 (2018).

[29] S. K. Anand and S. P. Singh, Phys. Rev. E **98**, 042501 (2018).

[30] Z. Mokhtari and A. Zippelius, Phys. Rev. Lett. **123**, 028001 (2019).

[31] A. Ghosh and A. J. Spakowitz, Soft Matter **18**, 6629 (2022).

[32] T. Eisenstecken, G. Gompper, and R. Winkler, Polymers **8**, 304 (2016).

[33] C. A. Philipps, G. Gompper, and R. G. Winkler, J. Chem. Phys. **157**, 194904 (2022).

[34] C. Nguyen, Y. Ozkan-Aydin, H. Tuazon, D. I. Goldman, M. S. Bhamla, and O. Peleg, Front. Phys. **9**, 734499 (2021).

[35] Y. Luo, J. Liu, Y. Gao, and Z. Lu, in *Intelligent Robotics and Applications*, edited by X. Zhang, H. Liu, Z. Chen, and N. Wang (Springer International, Cham, 2014), pp. 352–363.

[36] Joesinstructables, Snake robot, available at https://www.instructables.com/Snake-Robot-1/ (Autodesk, Inc., San Francisco, 2017).

[37] C. P. J. Wong and P. Choi, Comput. Mater. Sci. **155**, 320 (2018).

[38] J. M. Deutsch, J. Polymer Sci. B **50**, 379 (2012).

[39] J. M. Deutsch, Phys. Rev. E **83**, 051801 (2011).

[40] J. A. Anderson, J. Glaser, and S. C. Glotzer, Comput. Mater. Sci. **173**, 109363 (2020).

[41] J. D. Weeks, D. Chandler, and H. C. Andersen, J. Chem. Phys. **54**, 5237 (1971).

[42] See Supplemental Material at http://link.aps.org/supplemental/10.1103/PhysRevE.108.024606 for a sample video, additional numerical data, and detailed theoretical calculations, which includes Ref. [40].

[43] J. Rudnick and G. Gaspari, J. Phys. A: Math. Gen. **19**, L191 (1986).

[44] G. T. Barkema, D. Panja, and J. M. J. van Leeuwen, J. Stat. Mech. (2014) P11008.

[45] M. Doi and S. F. Edwards, *The Theory of Polymer Dynamics* (Clarendon, Oxford, 1986).

[46] A. Martín-Gómez, T. Eisenstecken, G. Gompper, and R. G. Winkler, Soft Matter **15**, 3957 (2019).

[47] M. S. E. Peterson, M. F. Hagan, and A. Baskaran, J. Stat. Mech. (2020) 013216.

[48] P. Baconnier, D. Shohat, C. H. López, C. Coulais, V. Démery, G. Düring, and O. Dauchot, Nat. Phys. **18**, 1234 (2022).

[49] E. Locatelli, V. Bianco, and P. Malgaretti, Phys. Rev. Lett. **126**, 097801 (2021).

[50] K. R. Prathyusha, S. Henkes, and R. Sknepnek, Phys. Rev. E **97**, 022606 (2018).